Reducing exciton-polaron annihilation in organic planar heterojunction solar cells

Bregt Verreet,[1,2,3,*] Ajay Bhoolokam,[1,4] Alyssa Brigeman,[5] Rijul Dhanker,[5] David Cheyns,[1] Paul Heremans,[1,4] Andre Stesmans,[2] Noel C. Giebink,[5] and Barry P. Rand[1,3,6]

[1]*imec, Kapeldreef 75, B-3001 Leuven, Belgium*

[2]*Semiconductor Physics Section, Department of Physics, Katholieke Universiteit Leuven, Celestijnenlaan 200D, B-3001 Leuven, Belgium*

[3]*Department of Electrical Engineering, Princeton University, Princeton, New Jersey 08544, USA*

[4]*ESAT, Katholieke Universiteit Leuven, Kasteelpark Arenberg 10, B-3001 Leuven, Belgium*

[5]*Department of Electrical Engineering, The Pennsylvania State University, University Park, Pennsylvania 16802, USA*

[6]*Andlinger Center for Energy and the Environment, Princeton University, Princeton, New Jersey 08544, USA*

(Received 6 February 2014; revised manuscript received 19 August 2014; published 4 September 2014)

We investigate the relationship between charge concentration, exciton concentration, and photocurrent generation in fullerene-containing heterojunction diodes. Impedance measurements on C_{60} diodes reveal a charge buildup at the C_{60}/bathocuproine (BCP) interface that can be swept out under reverse bias. In solar cell structures, a similar charge buildup is observed in dark conditions, and increases as a function of incident light intensity. Photoluminescence measurements reveal that the C_{60} exciton concentration is voltage dependent, explained via the process of exciton-polaron annihilation. This process has a negative impact on the generated photocurrent of the solar cells and thereby decreases the fill factor. A combination of electroabsorption, photoluminescence, and impedance measurements reveal a decrease in charge buildup and the associated exciton-polaron annihilation through the use of a BCP/3,4,9,10-perylenetetracarboxylic bis-benzimidazole/Ag cathode.

DOI: 10.1103/PhysRevB.90.115304 PACS number(s): 73.50.Gr, 73.50.Pz, 73.61.Wp

I. INTRODUCTION

At the core of organic photovoltaic cells is a photocurrent-generating heterojunction between donor and acceptor-type organic semiconductors. An improved understanding of the material properties has been crucial in realizing higher device performance. However, a more complete understanding of the physics behind organic solar cell operation is still needed to ensure continued progress. It is generally agreed that most of the photocurrent in such cells is generated through a four-step process, summarized by the following formula, which considers the external quantum efficiency (EQE) as a function of voltage (V) and wavelength λ:

$$\mathrm{EQE}(\lambda, V) = \eta_A(\lambda)\,\eta_{\mathrm{ED}}(\lambda)\,\eta_{\mathrm{CT}}(V)\,\eta_{\mathrm{CC}}(V). \quad (1)$$

First, a fraction $\eta_A(\lambda)$ of incident photons is absorbed, creating excitons. Next, excitons diffuse with exciton diffusion efficiency $\eta_{\mathrm{ED}}(\lambda)$ towards a donor/acceptor interface. This process is mainly wavelength dependent because of the separate diffusion processes in the donor and acceptor materials. At the donor/acceptor interface, charge transfer excitons are formed and split into free polarons with efficiency $\eta_{\mathrm{CT}}(V)$. Finally, the resulting polarons will be extracted with charge collection efficiency $\eta_{\mathrm{CC}}(V)$.

Much work on organic solar cell physics aims to unravel the detailed mechanism of one or more of these steps. Previous reports have, however, identified that the spectral response associated with excitons in the fullerene (C_{60} or C_{70}) acceptor is often voltage dependent, whereas the EQE in the donor material is constant with voltage [1–3], contradicting the simple model of Eq. (1). As both voltage dependent terms of Eq. (1) are considered equal for the donor and acceptor materials, one or more of the four factors in Eq. (1) must be adapted to include a dependence on *both* voltage and λ.

While this effect has been attributed to bulk ionization of excitons in C_{60} [1,4], we have recently suggested an alternative explanation [2], whereby $\eta_{\mathrm{ED}}(\lambda, V)$ is voltage dependent because a fraction of the excitons are quenched by exciton-polaron annihilation (EPA) before they reach the donor/acceptor interface [5]. In this process, an exciton transfers its energy to a nearby polaron via Förster resonance energy transfer (FRET). This process results in two effects which can be relevant for device performance. First, this effect will temporarily excite the polaron, until the excess energy is thermalized. In the case when the polaron was trapped, its excitation will temporarily increase the mobility in the layer. This mechanism was previously invoked to explain photomultiplication in Ni phthalocyanine/C_{60} devices under forward bias [6]. The second effect of the FRET is loss of an exciton. In organic light emitting devices, and especially in phosphorescent devices, a quantum efficiency rolloff is often observed at high current densities. This rolloff can be associated with EPA, triplet-triplet annihilation, electric field induced dissociation of excitons, and imbalanced charge injection [7–10]. Electron-polaron annihilation has also been studied in organic field effect transistors [11]. When the effect was studied in bulk heterojunction solar cells, it was found to be important at high light intensities [12]. Recently, it has been proposed that bimolecular recombination in poly(3-hexylthiophene) bulk heterojunctions can be caused by EPA instead of electron-hole Langevin recombination [13,14]. We previously found indications that in planar heterojunction solar cells, EPA limits cell efficiency even at low light intensity [2]. The effect would be more pronounced in planar heterojunctions compared to bulk heterojunctions because of higher exciton lifetimes in the unblended fullerene layers and a strong effect of injected space charge in the thin films.

*Author to whom correspondence should be addressed: bverreet@Princeton.EDU

The current density vs. voltage (*J-V*) slope observed in planar heterojunction solar cells depends strongly on the transport layers used at the cathode. For evaporated planar heterojunction cells, phenanthroline-based materials such as bathocuproine (BCP) are a common choice as a buffer layer between the acceptor C_{60} and cathode [15]. The main function of BCP is to protect the active layers from metal diffusion, preventing reaction of the metal with C_{60}, as this reaction would decrease the built-in field [16]. Furthermore, BCP blocks excitons [17] and functions as an optical spacer layer to best exploit optical interference effects. We previously found that a multilayer cathode buffer design [18–21], consisting of a 3,4,9,10-perylenetetracarboxylic bis-benzimidazole (PTCBI) layer in between BCP and Ag (as BCP/PTCBI/Ag), reduces the reverse-bias *J-V* slope, while simultaneously increasing the short-circuit current density (J_{sc}) and fill factor (FF) [2].

Here, we characterize C_{60}-based diodes and tris[4-(5-phenylthiophen-2-yl)phenyl]amine (TPTPA)/C_{60} solar cells to understand better the mechanism by which PTCBI influences EPA. We first investigate the presence of charging in diodes through impedance measurements and find that the BCP/PTCBI/Ag cathode significantly reduces charge buildup at the C_{60}/BCP interface compared to standard BCP/Ag cathodes. Electroabsorption (EA) measurements reveal that the BCP/PTCBI/Ag cathode has a lower built-in field, corresponding with less electron injection. Next, we characterize solar cell structures by impedance measurements under variable light intensity. A charge buildup is present even when no light bias is applied, due to charges injected by the cathode, and increases as a function of light intensity, due to photogenerated charges. The BCP/PTCBI/Ag cathode systematically decreases the charge buildup in both the diodes and the solar cells. Voltage dependent photoluminescence (PL) measurements reveal exciton quenching in C_{60} near open-circuit conditions, with a relative increase in quenching at high light intensities. This effect is not present with the BCP/PTCBI/Ag cathode. We propose a model of EPA at the C_{60}/BCP interface, which reproduces the measured PL spectra. The same model allows us to calculate the effect of EPA on the photocurrent. We find that the photocurrent of organic planar heterojunction solar cells is especially affected by EPA near operational conditions, thereby significantly decreasing the device performance of cells with a C_{60}/BCP interface.

II. EXPERIMENT

Substrate preparation and thin film deposition. Glass substrates coated with indium tin oxide (ITO, Thin Film Devices Inc., 140 nm, sheet resistance $<20\ \Omega\ \square^{-1}$) is cleaned by subsequent ultrasonic treatment in detergent, deionized water, acetone, and isopropanol, for 5 min each, followed by an ultraviolet-ozone treatment for 300 s. Poly(3,4-ethylenedioxythiophene):poly(styrenesulfonate) (PEDOT:PSS, HC Starck Clevios P) is deposited by spin coating for 60 s at 5000 rpm and annealed on a hot plate for 10 min at $T = 130$ °C. The samples are loaded in a vacuum chamber, where TPTPA, C_{60}, BCP, and PTCBI are evaporated at a rate of $\sim$1 Å s^{-1}. Deposition rates are determined from calibration of the film thickness, measured *ex situ* by spectroscopic ellipsometry (Sopra GESP-5). The ellipsometry data are also used to extract the dielectric constant ε_r for the materials, as the real part of $\varepsilon_r = n^2 - k^2$ will be determined by n in the limit of large wavelengths. All organic materials are purified before loading into the chamber by thermal gradient sublimation. The cathode, Ag, is deposited ($\sim 10^{-7}$ Torr, 3 Å s^{-1}, 100 nm), through a shadow mask, defining an active area of 0.134 cm^2.

Electrical characterization of the solar cells is performed with a Keithley 2602 measurement unit. Devices are measured in the dark and under 100 mW cm^{-2} AM1.5G simulated solar illumination (Abet), calibrated with a Fraunhofer certified photovoltaic cell. The impedance measurements are done with an E4980a precision LCR meter. Measurements are performed using the parallel model ($C_p - R_p$) with a small ac signal of 30 mV. During the impedance measurements, solar cells are light biased by laser light with $\lambda = 532$ nm (Roithner LaserTechnik RLDD532-50-5). The intensity of this light bias is calibrated by comparing the generated photocurrent J_{ph} at -2 V with the photocurrent generated at -2 V under 100 mW cm^{-2} AM1.5G conditions, according to the formula

$$x\ \text{sun} = J_{ph}(-2\ \text{V}, \lambda = 532\ \text{nm}) / J_{ph}(-2\ \text{V}, 100\ \text{mW AM1.5}).$$

For the *PL measurements*, solar cells are glass encapsulated in a nitrogen atmosphere. Excitation is applied with the same $\lambda = 532$ nm laser followed by a 700 nm cutoff short pass filter (Thorlabs). Figures 5(c) and 5(f) show the *J-V* characteristics of the cells in these conditions. The emission spectra are recorded using a triple-grating monochromator coupled to an intensified CCD camera (PI-MAX from Princeton Instruments). A voltage source (Keithley 2400) provides a voltage bias for the PL measurements.

Electroabsorption measurements are carried out using a Xe lamp and a monochromator with light incident on the device at an angle of $\sim 10°$ through the ITO anode and collected in reflection from the metal cathode (i.e., a double pass through the organic layer) via a calibrated Si photodiode. Electroabsorption spectra are recorded with a 0.45 V_{rms}, $f =$ 1 kHz ripple superimposed on the dc device bias and detected synchronously using a lock-in amplifier.

III. RESULTS

A. Diode characterization

We previously observed that the voltage dependence of the C_{60} photocurrent in planar heterojunction solar cells was influenced by the cathode architecture [2]. While we observed this effect in solar cells, we start our investigation here on simpler diode structures (thickness in nm):

$$\text{PEDOT} : \text{PSS}/\text{C}_{60}(30)/\text{BCP}(10)/\text{Ag} \quad \text{and}$$
$$\text{PEDOT} : \text{PSS}/\text{C}_{60}(30)/\text{BCP}(10)/\text{PTCBI}(4)/\text{Ag}.$$

Here, the PTCBI thickness was optimized for performance in the TPTPA/C_{60} solar cells discussed below.

The electrical impedance of the diodes in the dark was measured as a function of frequency in order to investigate

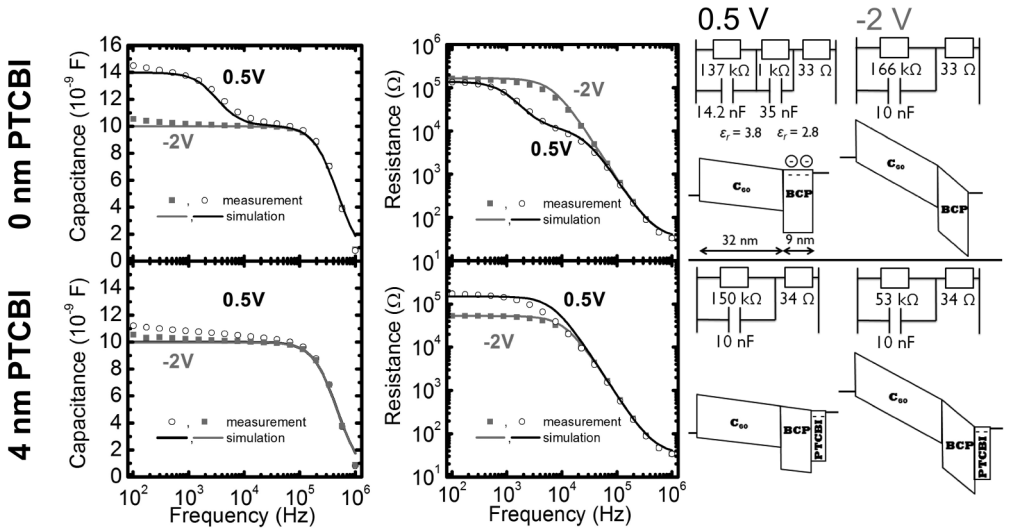

FIG. 1. Impedance measurement of C_{60} diodes in the dark with BCP/Ag cathode (upper graphs), or with BCP/PTCBI/Ag cathode (lower graphs). Capacitance (left) and resistance (middle) are measured as a function of frequency, at dc bias of 0.5 V (black circles) and 2 V (gray squares). Solid curves are simulation results, using the electronic circuits depicted at the right. The depicted energy diagrams at the right provide a schematic representation at the corresponding voltage.

charging within the diodes (see Fig. 1). These measurement results are compared with an electronic circuit simulation performed in PSPICE code, using equivalent circuits as depicted in Fig. 1 at the right. When the capacitance of the diode without PTCBI is measured at a bias of 0.5 V, a high capacitance $C_p > 14$ nF is found at low frequencies (Fig. 1, upper graph left, black curves). Assuming a relative dielectric constant $\varepsilon_r = 3.8$ for C_{60} and a diode area $A = 0.134$ cm^2, $t = 32$ nm can be calculated as the thickness of the layer which functions as a dielectric for this capacitance ($t = \varepsilon_r \varepsilon_0 A / C_p$). Since the C_{60} thickness is approximately 30 nm, this suggests that the C_{60} region remains largely depleted, while the ac signal charges the diode at the PEDOT:PSS anode and the C_{60}/BCP heterojunction [22]. Since it appears that for frequencies $f < 1$ kHz, charges at the C_{60}/BCP interface are modulated with the ac voltage, this implies that the BCP has relatively low resistance, extracted as 1 kΩ, because it is filled with charge injected by the Ag cathode under static conditions. At intermediate frequencies $f = 10^4$–10^5 Hz, electron transport is too slow within the BCP layer, and a geometric capacitance of 10 nF is measured. This corresponds to the capacitance of the complete C_{60}(32 nm)/BCP (9 nm, $\varepsilon_r = 2.8$) stack. At high frequencies, a 33 Ω series resistance determines the impedance.

When the same diode is biased at −2 V, the equivalent circuit simplifies to a model with the geometric capacitance as the only capacitor. The complete organic stack is depleted and the ac signal only charges PEDOT:PSS and Ag. A voltage dependent capacitance measurement at $f = 1$ kHz (Fig. 2, solid curve) reveals the capacitance peaks at 0.6 V with $C_p = 13$ nF. At reverse voltage, from 0 to −2 V, the measured capacitance corresponds to the geometric capacitance. This suggests that charges in the organic layers are swept out at reverse voltages. At forward voltages exceeding 0.8 V, both holes and electrons are injected into the diode and the capacitance increases substantially.

For diodes with BCP/PTCBI ($\varepsilon_r = 3.7$)/Ag cathodes, we found that the capacitance value remains close to the geometric capacitance over the whole voltage range from −2 to 0.5 V (Fig. 2, dotted curve). This suggests that with the additional PTCBI layer, charging at the C_{60}/BCP interface is suppressed.

To further explore the effect of the PTCBI layer on the charge density in the diodes, we performed electroabsorption experiments [23]. Here, the diodes are depleted in reverse bias and a small sinusoidal dither is superimposed on the bias, resulting in a change in C_{60} absorption, $\Delta A_{1\omega} \propto F_{\rm dc} F_{\rm ac} \sin(\omega t)$, that is nulled when the dc field within C_{60} is zero. Since the C-V data in Fig. 2 indicate that the devices are fully depleted in reverse bias (i.e., C is constant and equal to the geometric capacitance), the field in the C_{60} layer is uniform and linearly related to the applied bias for $V_{\rm applied} \leqslant 0$. In this region, the C_{60} EA peak at 2.48 eV [24] varies linearly

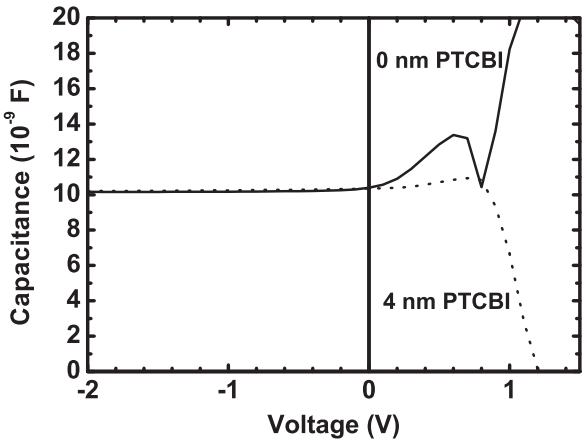

FIG. 2. Voltage dependent capacitance, measured at $f = 1$ kHz, of C_{60} diodes with either a BCP/Ag (solid curve) or a BCP/PTCBI/Ag cathode (dotted curve).

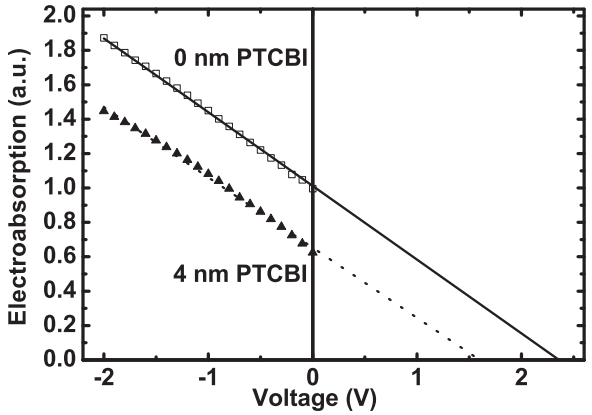

FIG. 3. Voltage dependent electroabsorption of C_{60} diodes with either a BCP/Ag (empty squares) or a BCP/PTCBI/Ag cathode (filled triangles). Linear extrapolation (solid and dotted curves) yields, respectively, $V_{bi} = 2.4$ V and $V_{bi} = 1.6$ V.

with bias as shown in Fig. 3 and can be extrapolated to the abscissa to yield the built-in voltage (V_{bi}) of the diodes [25]. It is evident from these linear fits that V_{bi} is decreased by approximately 0.8 V due to the addition of PTCBI. Because the anode injection barrier is the same for both devices, this indicates that the cathode injection barrier increases upon addition of PTCBI [26]. This implies that, at least in the dark at short circuit under thermal equilibrium, the electron density n in C_{60} decreases substantially upon addition of PTCBI according to $n = N_{LUMO}\exp[(E_F - E_{LUMO})/kT]$ because the difference between the lowest unoccupied molecular orbital (LUMO) energy and the Fermi level increases. Assuming relative dielectric constants $\varepsilon_{BCP} \approx 2.8$ and $\varepsilon_{C60} \approx 3.8$ for BCP and C_{60} respectively, only about 70% of the built-in potential drops across the C_{60} layer in each diode. The difference $E_{LUMO} - E_F$ in C_{60} adjacent to the BCP layer therefore increases by $\sim$0.55 eV with the addition of PTCBI, leading to a corresponding factor of $\exp(-0.55\ \text{eV}/kT) \sim 10^{-9}$ decrease in electron density at this location in the C_{60}.

B. Solar cell characterization

As a next step, we investigate solar cells with the following structures:

PEDOT : PSS/TPTPA(10)/C_{60}(30)/BCP(10)/Ag and

PEDOT : PSS/TPTPA(10)/C_{60}(30)/BCP(10)/PTCBI(4)/Ag.

In these TPTPA/C_{60} planar heterojunction solar cells, the addition of the thin PTCBI layer at the cathode has a pronounced effect. There is an increase in J_{sc} from 3.3 mA cm^{-2} without PTCBI to $J_{sc} = 4.6$ mA cm^{-2} with PTCBI. Moreover, the FF increases from 64% to 75%, leading to a relative increase of 60% in the power conversion efficiency ($\eta_P = 2.0\%$ to $\eta_P = 3.2\%$). This increase in photocurrent production is accompanied by a decrease in J-V slope at reverse voltages [see Fig. 4(a) and Table I]. When we previously applied the BCP/PTCBI/Ag cathode to diindenoperylene/C_{60} cells, we observed a similar increase in J_{sc} and FF, accompanied with a decreasing J-V slope at reverse bias [2]. In the same work, we saw similar, though less pronounced effects on Zn phthalocyanine/C_{60} cells with the BCP/PTCBI/Ag cathode architecture. We found that the effects were related to excitons in the C_{60} acceptor and that the ultrathin PTCBI layer has a negligible effect on the optical absorption of the solar cell.

As a comparison, we fabricated bulk heterojunction solar cells from the same donor:acceptor combination as in the planar heterojunction devices with the following structures:

MoO_3(5)/TPTPA : C_{60}(1 : 9,30)/BCP(10)/Ag and

MoO_3(5)/TPTPA : C_{60}(1 : 9,30)/BCP(10)/PTCBI(4)/Ag.

In contrast to the planar heterojunction case, the addition of the thin PTCBI layer at the bulk heterojunction cathode is detrimental to the device performance. Specifically, the FF

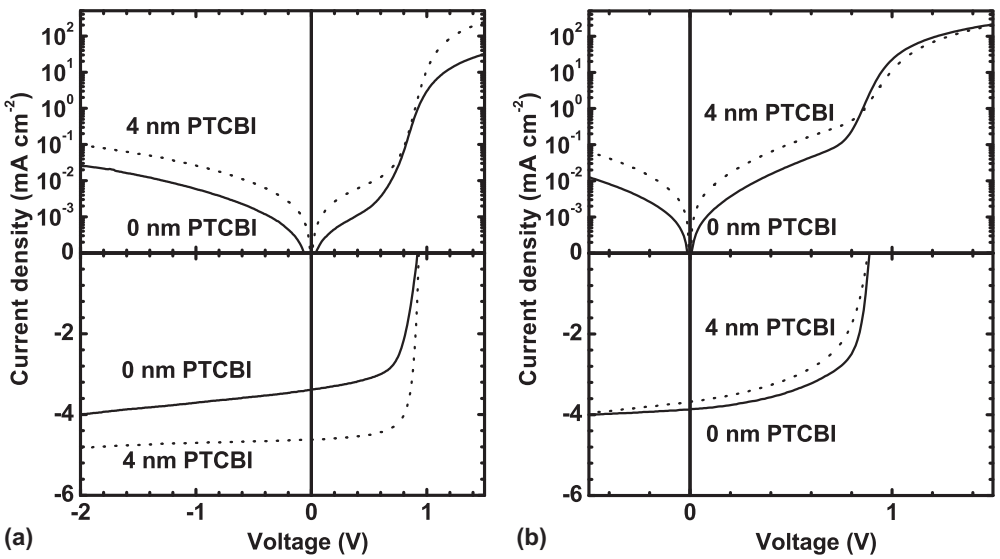

FIG. 4. Current density-voltage characteristics in the dark (upper graph) and under 100 mW cm^{-2} AM1.5G simulated solar illumination (lower graph) of (a) planar heterojunction TPTPA/C_{60} solar cells and (b) bulk heterojunction TPTPA:C_{60} solar cells with either BCP/Ag cathodes (solid curves) or with BCP/PTCBI/Ag cathodes (dotted curves).

TABLE I. J_{sc}, V_{oc}, FF, efficiency η_P, and J-V slope "$J(0.5\,V)/J(-2\,V)$" measured for 100 mW cm^{-2} AM1.5G simulated solar illumination. Series resistance R_s was derived by fitting dark curves from −1.5 to 1.5 V by the generalized Shockley equation.

Structure	J_{sc} (mA cm^{-2})	V_{oc} (V)	FF (%)	η_P (%)	R_s (Ω cm^2)	$\frac{J(0.5\,V)}{J(-2\,V)}$
TPTPA/C_{60}/BCP/Ag	3.3	0.92	64	1.98	13	0.78
TPTPA/C_{60}/BCP/ PTCBI (4)/Ag	4.6	0.93	75	3.22	1.7	0.93
TPTPA:C_{60}/BCP/Ag	3.9	0.89	61	2.05	2.2	
TPTPA:C_{60}/BCP/ PTCBI (4)/Ag	3.7	0.88	54	1.7	1.8	

decreases from 61% to 54% [Fig. 4(b) and Table I] and J_{sc} decreases from 3.9 mA/cm^2 to 3.7 mA/cm^2 when PTCBI is inserted, resulting in a power conversion efficiency drop of $\eta_P = 2.1\%$ to $\eta_P = 1.8\%$.

We continue our investigation via impedance measurements on the TPTPA/C_{60} solar cells. A voltage dependent capacitance measurement of a solar cell with a BCP/Ag cathode in the dark shows a geometric capacitance of $C_p = 8.8$ nF at −2 V [Fig. 5(a), gray solid curve]. This capacitance corresponds to that of a TPTPA (6.5 nm, $\varepsilon_r = 3.2$)/C_{60} (30 nm)/BCP(10 nm) stack. The capacitance increases with increasing voltage, with $C_p = 12.3$ nF at 0.5 V. As this trend is similar to the trend observed in the simpler diode structures, we ascribe this capacitance change to charging in the proximity of the C_{60}/BCP interface.

To investigate the charging of the solar cells under illumination, the cells were illuminated with $\lambda = 532$ nm laser light, a wavelength that allows for exclusive excitation of C_{60}. The power of the incident laser light was calibrated through the photocurrent generated at −2 V, as described in the Experiment section. For low to intermediate light intensities [Fig. 5(a), blue dotted curve and green dashed curve], the capacitance measurements yielded results similar to the C-V measurement in the dark over the voltage region from −2 to 0.5 V. At high light intensities, however, the capacitance increases [Fig. 5(a), black solid curve]. Similar light intensity dependent capacitance was previously reported in Cu phthalocyanine/C_{60}/BCP/Ag solar cells by Wang *et al.* [27]. In contrast, for the devices with a BCP/PTCBI/Ag cathode [Fig. 5(d)], no significant charging effects can be discerned at voltages below 0.5 V for the investigated intensity range.

Next, the exciton density in the solar cells is probed via voltage dependent PL measurements. Also here, C_{60} was excited selectively by $\lambda = 532$ nm laser illumination. The luminescence spectra were recorded at various solar cell voltage biases (Fig. S1 in the Supplemental Material) [28]. Figures 5(b) and 5(e) show the voltage dependence of the C_{60} luminescence peak height (integrated from $\lambda = 720$ nm to $\lambda = 800$ nm, normalized to the PL at −2 V at high intensities). For devices without PTCBI [Fig. 5(b), symbols], the C_{60} PL signal decreases by 20% from −2 to 0.5 V at low light intensities, while at high light intensities, this PL decrease amounts to 53%. In order to model the voltage dependence of the PL in Fig. 5(b), we first use the C-V data to calculate the charge in the organic layer. We assume that the capacitance measured at $f = 1$ kHz, for biases below 0.5 V, is representative of the capacitance caused by a unipolar buildup of charge in the organic layer in parallel with a geometric capacitance. We further assume that the organic layers are fully depleted at −2 V [geometric capacitance = $C(-2\,V)$]. In this case, the built-up charge in the organic layer $q_{org}(V)$ can be calculated by integrating the voltage dependent capacitance $C(W)$ of Fig. 5(a) over the range −2 V to voltage value V and subtracting the charging of the geometric capacitance:

$$q_{org}(V) = \int_{-2V}^{V} [C(W) - C(-2V)]\,dW. \tag{2}$$

The resulting charge is used as an input for an exciton diffusion equation:

$$\begin{aligned} G(x) + D\frac{dn(x,V)}{dx} - \frac{n(x,V)}{\tau} &= 0, \quad \text{when} \quad 0 < x < 29\ \text{nm}; \\ G(x) + D\frac{dn(x,V)}{dx} - \frac{n(x,V)}{\tau} - K_{XP}\frac{q_{org}(V)}{Al}n(x,V) &= 0 \quad \text{when} \quad 29 \leqslant x < 30\ \text{nm}, \end{aligned} \tag{3}$$

where $n(x,V)$ represents the exciton density in C_{60}, $G(x)$ is the photogeneration of excitons calculated by the transfer-matrix method, and $\tau = 250$ ns is the exciton lifetime in C_{60} [29]. Fitting the photocurrent in Fig. 4(a) at −2 V bias results in an exciton diffusion length $L_D = 25$ nm for C_{60}, corresponding to a diffusivity $D = 2.5 \times 10^{-9}$ m^2 s^{-1}. The model assumes 100% efficient exciton dissociation at the TPTPA/C_{60} interface, at $x = 0$ nm, and exciton-polaron annihilation proportional to $q_{org}(V)$ by a thin charge sheet at the C_{60}/BCP interface, at $x = 30$ nm. This exciton annihilation process was implemented by introducing a fourth term to Eq. (3) for near the C_{60}/BCP interface, between $x = 29$ nm and $x = 30$ nm (thickness $l = 1$ nm). Integrating $n(x,V)$ over x and device area A yields the number of excitons $N(V)$, which is proportional to the photoluminescence PL(V):

$$\mathrm{PL}(V) = \frac{N(V)}{N(-2V)}\mathrm{PL}(-2V). \tag{4}$$

The C-V data of Fig. 5(a) for low, intermediate, and high light intensity were inserted into Eqs. (3) and (4) in order to obtain the respective solid curves shown in Fig. 5(b), using 0.6×10^{-10}, 1.2×10^{-10}, and 1.4×10^{-10} cm^3 s^{-1} as respective fitting parameters for K_{XP}.

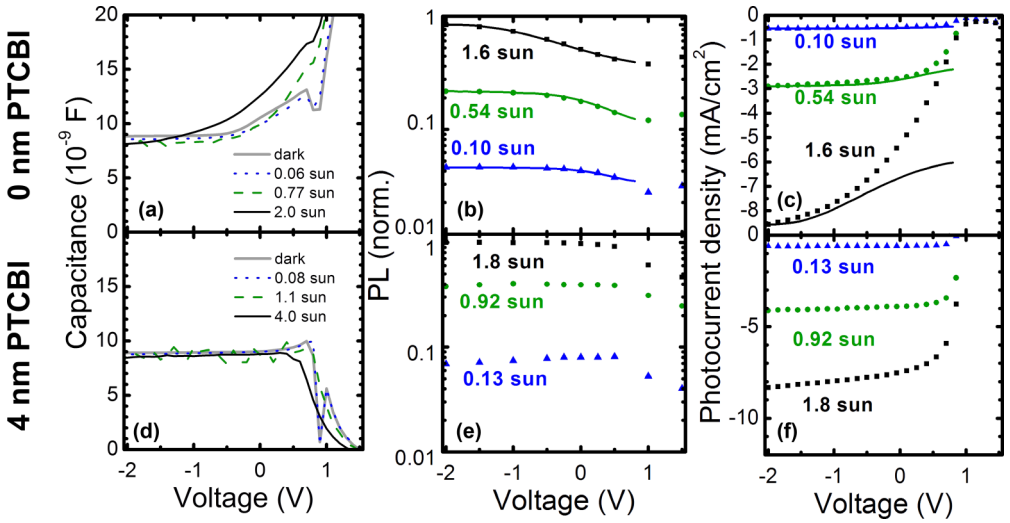

FIG. 5. (Color online) Characterization of TPTPA/C_{60} based solar cells, with either a BCP/Ag (a), (b), (c) or BCP/PTCBI/Ag (d), (e), (f) cathode. Light conditions are varied over high (black), intermediate (green), and low intensities (blue), while the gray solid lines represent dark measurement results. Light bias was performed by a $\lambda = 532$ nm laser; indicated intensities are for equivalent photocurrent production (see text). (a), (d) Voltage dependent capacitance measurement at $f = 1$ kHz. (b), (e) Voltage dependent photoluminescence measurement (symbols). Solid curves in (b) are modeling results, derived from the capacitance measurements. (c), (f) Photocurrent density measurement as a function of voltage (symbols). Solid curves in (c) represent the modeled loss associated with EPA, as described in the text.

During the photoluminescence experiment, we measured the photocurrent densities, defined as illuminated current density minus the dark current density [Figs. 5(c) and 5(f)]. The solid curves in Fig. 5(c) represent the photocurrent loss associated with EPA, $\eta_{ED}(V)/\eta_{ED}(-2\,V) \times J(-2\,V)$, where $\eta_{ED}(V)$ and $\eta_{ED}(-2\,V)$ are modeled using the same parameters as the PL model, and $J(-2\ V)$ is measured. For the solar cell without PTCBI, the measured photocurrent drops 20% from -2 to 0.5 V at low light intensities, whereas our model predicts that $\eta_{ED}(V)$ drops 10% because of EPA. At high intensities, the measured photocurrent drops 64% from -2 to 0.5 V. According to our model, EPA has a strong effect here, with a 28% $\eta_{ED}(V)$ drop in this voltage range. With PTCBI, the capacitance reveals no charging over the studied voltage range, and as a consequence the photocurrent shows a decreased slope, with only a 5% and 19% drop in photocurrent from -2 to 0.5 V for low and high light intensity, respectively.

IV. DISCUSSION

The capacitance measurements reveal the presence of charges nearby the C_{60}/BCP interface in the case of BCP/Ag cathodes, both in C_{60}-based diodes and in TPTPA/C_{60} solar cells, an aspect likely associated with gap states. Wang *et al.* previously reported that Ag induced gap states are present in both BCP and C_{60} within Ag/BCP/C_{60} stacks [30]. Injected electrons fill up these gap states, thereby reducing the LUMO offset at BCP/C_{60} from 1.4 to 0.7 eV. In their reported Ag/BCP/C_{60} stack, these gap states in C_{60} were only found for BCP thicknesses under 5 nm. We can, however, assume that Ag will penetrate deeper into the organic layers when it is evaporated as a top contact [31], as in our case. Moreover, a recent publication revealed that gap states are present at the C_{60}/BCP interface even before Ag deposition [32].

The capacitance measurements further revealed that BCP/PTCBI/Ag cathodes lead to less charge injection in the diodes and solar cells. This result is in line with our previous speculation that the PTCBI layer diminishes the electron density at the C_{60}/BCP contact [2]. A strong dipole ($\geq$0.9 eV) was previously observed at the BCP/Ag contact, which ensures a high electron density within the BCP layer [33,34]. The cumulative dipole over PTCBI/Ag ($\leq$0.2 eV) [35,36] and BCP/PTCBI (0.4 eV) [37,38] would be less. This decrease in total vacuum shift over BCP/PTCBI/Ag compared to BCP/Ag eventually results in a decreased electron density at the C_{60}/BCP interface and the decreased V_{bi} measured by electroabsorption (cf. Fig. 3).

It can further be noticed that the insertion of the 4 nm PTCBI layer into the diode structure does not affect the geometric capacitance measured at -2 V (Figs. 1 and 5, left graphs, gray curves). It has been reported that Ag deposition results in polaron filled gap states in PTCBI [35,36]. Possibly, the 4 nm PTCBI layer becomes highly doped in this way, ensuring it cannot discharge, even at reverse voltages of -2 V.

Our PL measurements on devices with BCP/Ag cathode indicate no voltage dependence from -2 to -0.5 V at low light intensity. This contradicts a previously stated theory that the nonzero *J-V* slope in this voltage region would be caused by bulk ionization of excitons in C_{60} [1,4]. That theory would predict more dissociation of excitons at reverse voltages, and thus *lower* exciton concentrations. Our *C-V* data indicate no charging from -2 to -0.5 V and hence EPA cannot be responsible for the *J-V* slope in this voltage region either. The exact physics behind the fullerene-related nonzero *J-V* slope and photomultiplication effects [3,39] at high reverse voltages thus currently remains unresolved. We do, however, observe a decrease in PL intensity from -0.5 to 1 V for low

light intensity and from −2 to 1 V for high light intensities. We successfully modeled this voltage dependence of the PL by EPA, using realistic values for the exciton-polaron interaction $K_{XP} = 0.6 - 1.4 \times 10^{-10}\,\mathrm{cm^3\,s^{-1}}$. When this built-up charge is eliminated in solar cells with a BCP/PTCBI/Ag cathode, the PL intensity becomes voltage independent at voltages below 0.5 V. The mechanism of EPA is thus able to explain the relation between charge density and photoluminescence of the investigated solar cells.

These results can now be used to provide insight into the planar heterojunction solar cell *J-V* graphs depicted in Fig. 4(a). The dark curves reveal that the forward current increases after the addition of a PTCBI layer, indicated by the series resistance R_s which decreases from 13 to 1.7 Ω cm^{-2}. Given the changes observed for electron concentration in C_{60}, the opposite trend could have been expected. But while the addition of PTCBI does lead to a lower electron concentration in C_{60}, it also eliminates the barrier at the BCP/Ag interface, which could explain the decrease in R_s. With respect to the illuminated curves, our model predicts a 10% and 28% decrease in $\eta_{ED}(V)$ at 0.5 V for low and high light intensities, respectively. The photocurrent of BCP/Ag-based devices is thus strongly affected by EPA near operational conditions. We now also understand that PTCBI decreases the steady-state polaron concentration in C_{60} which results in a less voltage dependent exciton population, enhancing FF and J_{sc}. Figure S2 in the Supplemental Material [28] compares the absolute photoluminescence of devices at 0 V with and without PTCBI, supporting the claim that the J_{sc} increase achieved by the BCP/PTCBI/Ag cathode is indeed associated with a higher steady-state exciton concentration. However, the higher PL and J_{sc} cannot be fully explained by EPA. Analysis of Fig. 4(a) reveals that at −2 V, devices with PTCBI produce $J(-2\ \mathrm{V}) = 4.8\ \mathrm{mA\ cm^{-2}}$, compared to $J(-2\ \mathrm{V}) = 4.0\ \mathrm{mA\ cm^{-2}}$ for devices without PTCBI. At −2 V, EPA should be absent as charge is no longer present in the organic layers. Assuming EPA sources from filled traps near the C_{60}/BCP interface, we propose that this additional contribution when no charge is present may source from empty traps that become filled through Dexter or Förster energy transfer from an exciton exciting an electron in its ground state [40].

The impact of EPA on planar heterojunction cells has the unexpected consequence that a decrease in built-in voltage leads to an improved performance. We observed the opposite, more conventional trend, when the BCP/PTCBI/Ag cathode was deposited on a TPTPA:C_{60} bulk heterojunction: The FF and J_{sc} decreased compared to devices with a BCP/Ag cathode [Fig. 4(b), Table I]. In bulk heterojunction solar cells, the effect of EPA is expected to be less pronounced as the exciton concentrations are lower, because of faster exciton dissociation. Bulk heterojunction solar cells, however, rely more on the built-in voltage for charge collection than planar heterojunction cells, where the electron blocking donor layer and hole blocking acceptor layer ensure an intrinsic selectivity for charge extraction [41]. In depleted bulk heterojunctions, the carrier with the longest drift length $L_{dr} = \mu\tau F$ determines the current-voltage curve, where μ is mobility, τ is charge carrier lifetime, and F is the electrical field in the device [42,43]. A decreased built-in voltage results in a decreased field F, which in turn decreases charge collection and therefore increases charge recombination in bulk heterojunction solar cells [44].

V. CONCLUSION

Capacitance measurements on C_{60} diodes and TPTPA/C_{60} planar heterojunction solar cells revealed a charge buildup from injection by the BCP/Ag cathodes, even under dark conditions. At reverse voltages, the charges, which are likely trapped on Ag induced defects in C_{60} and BCP, are swept out of the device. Voltage dependent PL measurements reveal that the space charge quenches C_{60} excitons. This exciton-polaron annihilation subsequently decreases the number of excitons in C_{60} that can reach the donor/acceptor interface, indicated by $\eta_{ED}(\lambda, V)$. This effect enhances the voltage dependence of the photocurrent generation and hence negatively affects FF.

The use of BCP/PTCBI/Ag cathodes strongly reduces the observed charge buildup and associated exciton-polaron annihilation. According to electroabsorption measurements, this can be attributed to a higher Fermi level-LUMO offset at the C_{60}/BCP heterojunction. We therefore conclude that by decreasing exciton-polaron annihilation, the lower built-in field of the BCP/PTCBI/Ag cathode counterintuitively results in planar heterojunction devices with higher FF and J_{sc}.

ACKNOWLEDGMENTS

The research leading to these results has received funding from the European Community's Seventh Framework Programme (FP7/2007-2013) under Grant Agreement No. 287818 of the X10D project and from the European Community's ERC Advanced Grant No. 320680 (EPOS CRYSTALLI). B.V. acknowledges funding from a KU Leuven PDM Kort Scholarship and through the Belgian American Educational Foundation. The authors want to thank Erwin Vandenplas and Kjell Cnops for processing support and a reviewer for useful comments and suggestions.

[1] W.-I. Jeong, Y. E. Lee, H.-S. Shim, T.-M. Kim, S.-Y. Kim, and J.-J. Kim, Adv. Funct. Mater. **22**, 3089 (2012).

[2] B. Verreet, P. E. Malinowski, B. Niesen, D. Cheyns, P. Heremans, A. Stesmans, and B. P. Rand, Appl. Phys. Lett. **102**, 043301 (2013).

[3] W. Tress, K. Leo, and M. Riede, Phys. Status Solidi RRL **7**, 401 (2013).

[4] C. K. Renshaw, J. D. Zimmerman, B. E. Lassiter, and S. R. Forrest, Phys. Rev. B **86**, 085324 (2012).

[5] J. C. Bolinger, M. C. Traub, T. Adachi, and P. F. Barbara, Science **331**, 565 (2011).

[6] J. Reynaerts, V. I. Arkhipov, P. Heremans, and J. Poortmans, Adv. Funct. Mater. **16**, 784 (2006).
[7] Y. Luo, H. Aziz, G. Xu, and Z. D. Popovic, Chem. Mater. **19**, 2288 (2007).
[8] R. H. Young, C. W. Tang, and A. P. Marchetti, Appl. Phys. Lett. **80**, 874 (2002).
[9] J. W. Kang, S.-H. Lee, H. D. Park, W.-I. Jeong, K.-M. Yoo, Y.-S. Park, and J.-J. Kim, Appl. Phys. Lett. **90**, 223508 (2007).
[10] N. C. Giebink and S. R. Forrest, Phys. Rev. B **77**, 235215 (2008).
[11] N. H. Hansen, C. Wunderlich, A. K. Topczak, E. Rohwer, H. Schwoerer, and J. Pflaum, Phys. Rev. B **87**, 241202 (2013).
[12] J. M. Hodgkiss, S. Albert-Seifried, A. Rao, A. J. Barker, A. R. Campbell, R. A. Marsh, and R. H. Friend, Adv. Funct. Mater. **22**, 1567 (2012).
[13] L. Tzabari, V. Zayats, and N. Tessler, J. Appl. Phys. **114**, 154514 (2013).
[14] A. J. Ferguson, N. Kopidakis, S. E. Shaheen, and G. Rumbles, J. Phys. Chem. C **112**, 9865 (2008).
[15] P. Peumans and S. R. Forrest, Appl. Phys. Lett. **79**, 126 (2001).
[16] H. Gommans, B. Verreet, B. P. Rand, R. Müller, J. Poortmans, P. Heremans, and J. Genoe, Adv. Funct. Mater. **18**, 3686 (2008).
[17] S. Wang, T. Sakurai, K. Komatsu, and K. Akimoto, J. Cryst. Growth **378**, 415 (2013).
[18] B. E. Lassiter, G. Wei, S. Wang, J. D. Zimmerman, V. V. Diev, M. E. Thompson, and S. R. Forrest, Appl. Phys. Lett. **98**, 243307 (2011).
[19] T. Zhuang, Z. Su, Y. Liu, B. Chu, W. Li, J. Wang, F. Jin, X. Yan, B. Zhao, F. Zhang, and D. Fan, Appl. Phys. Lett. **100**, 243902 (2012).
[20] H.-W. Lin, H.-W. Kang, Z.-Y. Huang, C.-W. Chen, Y.-H. Chen, L.-Y. Lin, F. Lin, and K.-T. Wong, Org. Electron. **13**, 1925 (2012).
[21] A. N. Bartynski, C. Trinh, A. Panda, K. Bergemann, B. E. Lassiter, J. D. Zimmerman, S. R. Forrest, and M. E. Thompson, Nano Lett. **13**, 3315 (2013).
[22] N. D. Nguyen and M. Schmeits, Phys. Status Solidi **203**, 1901 (2006).
[23] T. M. Brown, J. S. Kim, R. H. Friend, F. Cacialli, R. Daik, and W. J. Feast, Appl. Phys. Lett. **75**, 1679 (1999).
[24] S. Kazaoui, N. Minami, Y. Tanabe, H. J. Byrne, A. Eilmes, and P. Petelenz, Phys. Rev. B **58**, 7689 (1998).
[25] I. H. Campbell, J. P. Ferraris, T. W. Hagler, M. D. Joswick, I. D. Parker, and D. L. Smith, Polymer. Adv. Tech. **8**, 417 (1997).
[26] T. M. Brown, R. H. Friend, I. S. Millard, D. J. Lacey, J. H. Burroughes, and F. Cacialli, Appl. Phys. Lett. **77**, 3096 (2000).
[27] J. C. Wang, X. C. Ren, S. Q. Shi, C. W. Leung, and P. K. L. Chan, Org. Electron. **12**, 880 (2011).
[28] See Supplemental Material at http://link.aps.org/supplemental/10.1103/PhysRevB.90.115304 for wavelength resolved luminescence spectra and a direct comparison of photoluminescence of devices with and without PTCBI.
[29] T. W. Ebbesen, Y. Mochizuki, K. Tanigaki, and H. Hiura, Europhys. Lett. **25**, 503 (1994).
[30] S. Wang, T. Sakurai, R. Kuroda, and K. Akimoto, Appl. Phys. Lett. **100**, 243301 (2012).
[31] S. Fladischer, A. Neuhold, E. Kraker, T. Haber, B. Lamprecht, I. Salzman, R. Resel, and W. Grooger, ACS Appl. Mater. Interfaces **4**, 5608 (2012).
[32] Y. Nakayama, T. L. Nguyen, Y. Ozawa, S. Machida, T. Sato, H. Tokairin, Y. Noguchi, and H. Ishii, Adv. Energy Mater. **4**, 1301354 (2014).
[33] T. Sakurai, S. Toyoshima, H. Kitazume, S. Masuda, H. Kato, and K. Akimoto, J. Appl. Phys. **107**, 043707 (2010).
[34] K. Akaike and Y. Kubozono, Org. Electron. **14**, 1 (2013).
[35] N. J. Watkins, G. P. Kushto, and A. J. Mäkinen, J. Appl. Phys. **104**, 013712 (2008).
[36] I. G. Hill, J. Schwartz, and A. Kahn, Org. Electron. **1**, 5 (2000).
[37] H. Vázquez, W. Gao, F. Flores, and A. Kahn, Phys. Rev. B **71**, 041306 (R) (2005).
[38] I. G. Hill, D. Milliron, J. Schwartz, and A. Kahn, Appl. Surf. Sci. **166**, 354 (2000).
[39] J. Huang and Y. Yang, Appl. Phys. Lett. **91**, 203505 (2007).
[40] M. Pope and C. Swenberg, *Electronic Processes in Organic Crystals and Polymers* (Oxford University Press, New York, 1999).
[41] D. Cheyns, J. Poortmans, P. Heremans, C. Deibel, S. Verlaak, B. P. Rand, and J. Genoe, Phys. Rev. B **77**, 165332 (2008).
[42] R. S. Crandall, J. Appl. Phys. **53**, 3350 (1982).
[43] R. A. Street, A. Krakaris, and S. R. Cowan, Adv. Funct. Mater. **22**, 4608 (2012).
[44] B. Zimmerman, M. Glatthaar, M. Niggemann, M. Riede, and A. Hinsch, Thin Solid Films **493**, 170 (2005).